## ARTICLE

Check for updates

Double-diffusive mixing makes a small contribution to the global ocean circulation

Carine G. van der Boog [1✉], Henk A. Dijkstra[2], Julie D. Pietrzak[1] & Caroline A. Katsman [1]

Double-diffusive processes enhance diapycnal mixing of heat and salt in the open ocean. However, observationally based evidence of the effects of double-diffusive mixing on the global ocean circulation is lacking. Here we analyze the occurrence of double-diffusive thermohaline staircases in a dataset containing over 480,000 temperature and salinity profiles from Argo floats and Ice-Tethered Profilers. We show that about 14% of all profiles contains thermohaline staircases that appear clustered in specific regions, with one hitherto unknown cluster overlying the westward flowing waters of the Tasman Leakage. We estimate the combined contribution of double-diffusive fluxes in all thermohaline staircases to the global ocean's mechanical energy budget as 7.5 GW [0.1 GW; 32.8 GW]. This is small compared to the estimated energy required to maintain the observed ocean stratification of roughly 2 TW. Nevertheless, we suggest that the regional effects, for example near Australia, could be pronounced.

[1] Environmental Fluid Mechanics, Civil Engineering and Geosciences, Delft University of Technology, Delft, The Netherlands. [2] Institute for Marine and Atmospheric research Utrecht, Utrecht University, Utrecht, The Netherlands. ✉email: c.g.vanderboog@tudelft.nl

Double diffusion arises in the ocean when either the temperature- or salinity-induced stratification is statically unstable, while the overall density stratification is statically stable[1]. Two regimes of double diffusion are distinguished: the salt-finger regime characterized by a destabilizing salinity stratification, and the diffusive-convective regime with a destabilizing temperature stratification. The release of potential energy stored in the stratification of the unstable component drives the double-diffusive mixing, resulting in a counter-gradient buoyancy flux that restratifies the water column[2]. Another aspect typical for double-diffusive mixing is an inequality between the density components of the resulting vertical salt and heat fluxes; the density flux ratio $\gamma = F_T/F_S \neq 1$, where F_T is the vertical heat flux and F_S is the vertical salt flux[3].

Ocean general circulation models that incorporate parameterizations of double-diffusive mixing indicate that it induces a weakening of the ocean's meridional overturning circulation[4–6]. This decrease could either arise from the counter-gradient diapycnal mixing or from the modification of water masses through the differential vertical fluxes of heat and salt. First, the diapycnal mixing caused by double diffusion contributes to the mechanical energy budget in the deep ocean. In total, ~2 TW is required to maintain the abyssal stratification[7–9]. Double-diffusive mixing can occur in the open ocean and enhances interior mixing locally[2]. However, the magnitude of its resulting contribution to the global mechanical energy budget is so far unknown.

Second, observations indicate that the double-diffusive vertical fluxes of heat and salt could modify oceanic properties[10,11]. For example, the waters in the southern Indian Ocean became more susceptible to double diffusion over the last decades[10]. Observations[10] indicated that this could lead to stronger double-diffusive fluxes, which in turn provides an explanation for the observed changes in the water masses in this period. Also in the Mediterranean Sea, the vertical transport of heat and salt between the Levantine Intermediate Water and Mediterranean Deep Water seems to be dominated by double-diffusive fluxes[12]. Over the past decades, these fluxes increased the salinity of the Mediterranean Deep Water, which in turn affected the salt and heat input into the Atlantic Ocean[11]. Furthermore, due to the inequality of the strength of the vertical heat and salt fluxes associated with double diffusion, it is thought to be the major consumer of spiciness in the ocean[13,14].

Although many studies have highlighted the importance of double-diffusive mixing in the ocean, an observationally based analysis of the impact of these processes on the global ocean circulation is lacking. In this study, we analyze the global distribution of thermohaline staircases, which arise from double-diffusive processes. Thermohaline staircases are stepped structures in the temperature and salinity stratification consisting of a sequence of subsurface mixed layers separated by thin interfaces with sharp temperature and salinity gradients. The mixed-layer heights of thermohaline staircases range from several meters in the Arctic Ocean[15,16] to several hundreds of meters in the Tyrrhenian Sea and Black Sea[2]. In contrast to the microstructure of the double-diffusive mixing itself, the vertical length scales of the mixed layers of thermohaline staircases are larger so that they can be captured by Argo floats and Ice-Tethered Profilers[17,18] (see "Methods"). Based on our global distribution of thermohaline staircases[19], we compute the effective diffusivity of heat and salt in each step of a thermohaline staircase and use that to quantify the total contribution of double-diffusive mixing to the global mechanical energy budget.

Results

The global distribution of thermohaline staircases. The global distribution of thermohaline staircases obtained using the methods outlined in the "Methods" section, indicates that thermohaline staircases are formed in specific regions depending on regional water-mass characteristics (Fig. 1). In total, the global dataset comprises 39,469 profiles with thermohaline staircases in the salt-finger regime ($n^{SF} = 8.1\%$ of all 487,493 profiles) and 31,053 profiles with thermohaline staircases in the diffusive-convective regime ($n^{DC} = 6.4\%$ of all profiles).

In general, thermohaline staircases in the diffusive-convective regime occur at high latitudes where fresh and cold surface waters overlie warmer and more saline waters. Especially the Canada Basin that is located within the Arctic Ocean is known for its persistent occurrence of thermohaline staircases[15,16]. There, thermohaline staircases with a high number of steps are observed (dark blue areas in Fig. 1). Previous studies estimated the double-diffusive upward heat transport at 0.004–0.3 W m^{-2}, which is an order of magnitude smaller than the mean surface mixed-layer heat flux[15,20]. In line with this estimate, we find an upper bound of the average heat fluxes of 0.5 W m^{-2} (at 135°W–145°W, 75°N–80°N, Fig. 2a). Besides the Canada Basin, other regions in the Arctic Ocean and Southern Ocean also reveal the presence of thermohaline staircases in the diffusive-convective regime[21–24].

At lower latitudes, double diffusion is predominantly in the salt-finger regime (red in Fig. 1). Using the automated detection algorithm, we identify thermohaline staircases in all well-known formation regions: in the western tropical Atlantic Ocean[17,25], the Caribbean Sea[26,27], below the Mediterranean outflow[28], within the Mediterranean Sea[12,29] and along the equator[30]. These
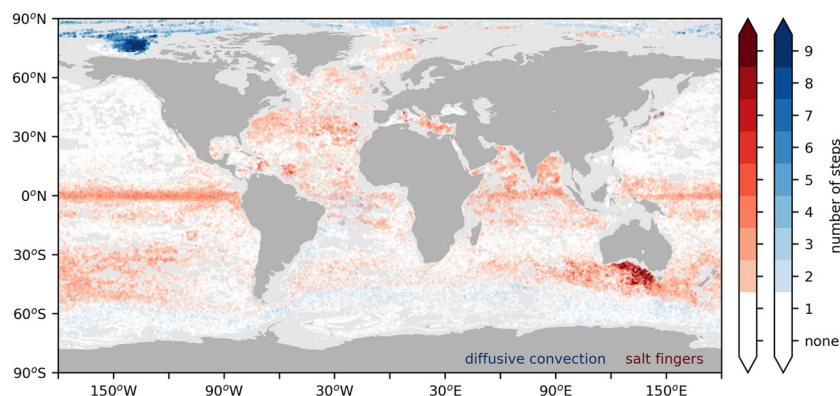

Fig. 1 Global distribution of the occurrence of thermohaline staircases based on global dataset of Argo floats and Ice-Tethered Profiles using the detection algorithm[19]. For each profile, the number of steps within thermohaline staircases in the salt-finger regime (red dots) and diffusive-convective regime (blue dots) is plotted. Profiles with the largest numbers of steps are plotted last for clarity.
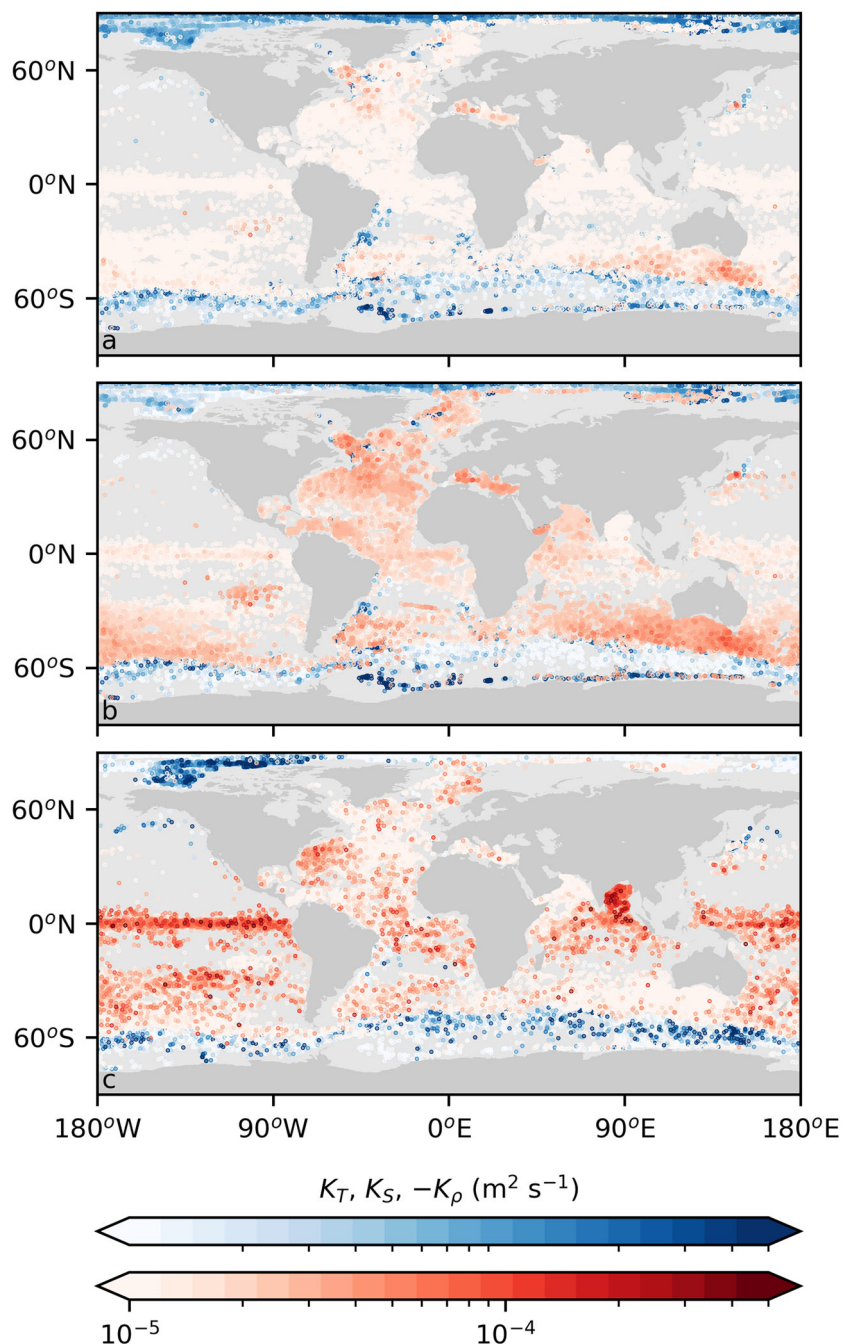
Fig. 2 Effective diffusivities (per profile) computed in each profile with a thermohaline staircase. For each profile, the average diffusivities per staircase in the salt-finger regime (red dots) and diffusive-convective regime (blue dots) are plotted. Panels show the average effective diffusivity of **a** heat (K_T) and **b** salt (K_S), and **c** buoyancy (K_ρ) per profile.

thermohaline staircases have, in general, thicker mixed layers and interfaces than staircases in the diffusive-convective regime[2], which allows for more accurate estimates of the temperature and salinity steps across interfaces[19]. Using a previous empirical estimate[31], we obtain an average effective diffusivity of salt of $K_S^{\mathrm{SF}} = 1.92 \times 10^{-5}\ \mathrm{m^2\,s^{-1}}$ [$2.5 \times 10^{-7}\ \mathrm{m^2\,s^{-1}}$; $1.0 \times 10^{-4}\ \mathrm{m^2\,s^{-1}}$], where the values between brackets correspond to the 2.5- and 97.5-percentile ranges (Fig. 2b).

Besides these well-known regions with thermohaline staircases, the global analysis presented here also reveals a newly discovered staircase region in the Great Australian Bight (Figs. 1 and 3a, b). There, the warm and saline Subtropical Surface Water overlies the cold and fresh Antarctic Intermediate Water (Fig. 3a, b). This

interface is susceptible to double-diffusive mixing with Turner angles varying between $45° < \mathrm{Tu} < 90°$[32]. As expected the mixed layers of the staircases are located at this interface (Fig. 3c). Thermohaline staircases appear abundant in this region (32°S–42°S, 125°E–145°E): in total, 62% of the 2241 profiles contain staircases (Fig. 3d). The alignment of the temperature and salinity data of each mixed-layer (alignment in Fig. 3e) indicates that the mixed-layer properties and vertical structure of the staircases are similar across multiple profiles. To gain insight in the lateral coherence of these similarities of the properties, we quantify using the aligned data points as an example (red dots in Fig. 3e). We obtain a lateral coherence over a region of several hundreds of kilometers that persisted for almost 2 years, which is
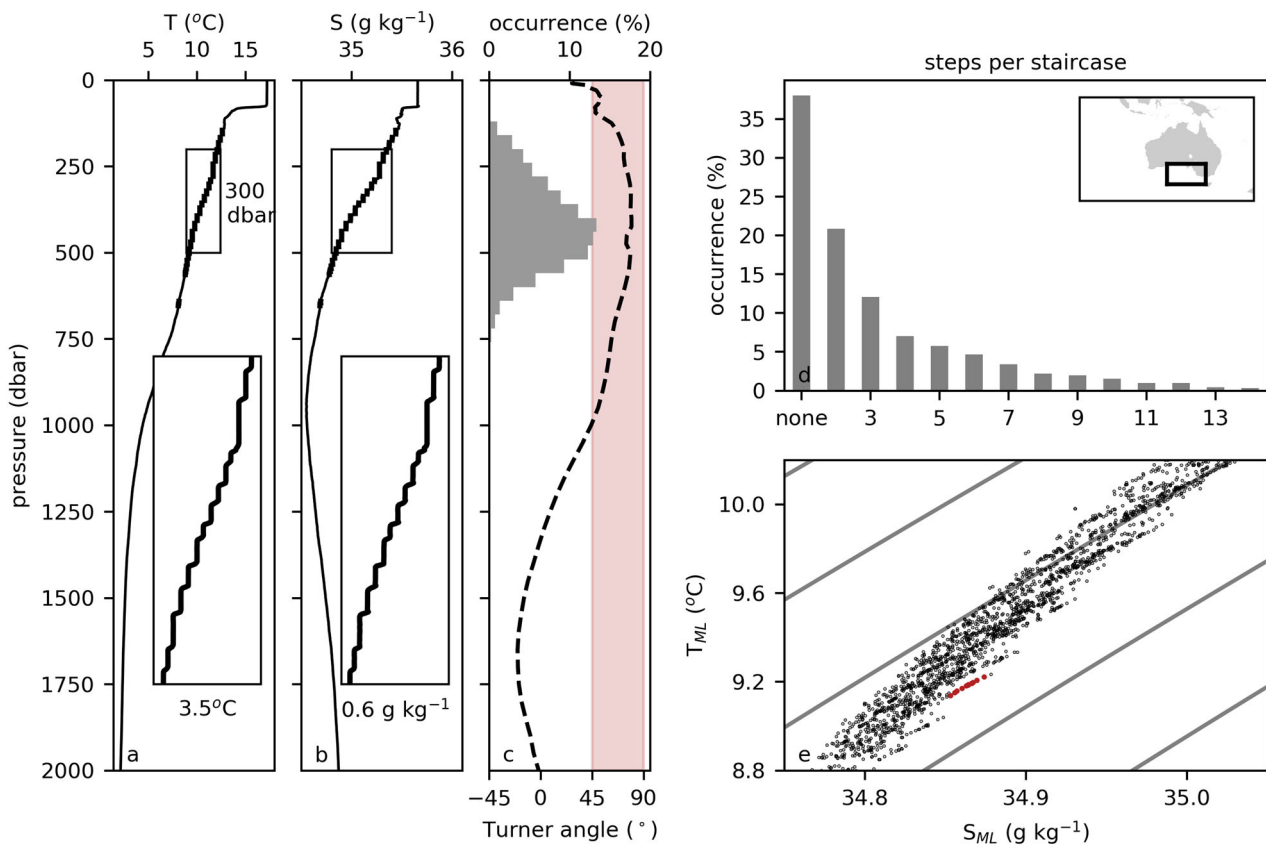
Fig. 3 Properties of thermohaline staircases in the Great Australian Bight (32°S–42°S, 125°E–145°E). a Example temperature and **b** salinity profile with a thermohaline staircase obtained by an Argo float (float-id: 5905189) at 37.6°S, 135.1°E on 8 April 2019. The inlays show a zoom of the profiles between 200 and 500 dbar. **c** Distribution of mixed layers over depth (gray bars) and the average Turner angle[32] in the Great Australian Bight (dashed line). The red shading indicates Turner angles corresponding to the salt-finger regime (45° < Tu < 90°). **d** Distribution of number of steps per profile in percentage. **e** Scatter plot of the temperature and salinity of the mixed layers of the detected staircases, where red dots indicate mixed layers that are used to compute the lateral coherence. Data in panels **c**, **d**, and **e** is obtained between 23 April 2007 and 13 May 2020. Inlay in **d** shows the considered region.

similar to what is seen in other major staircase regions[15,25]. The slopes of these aligned points correspond to the density flux ratio and confirm a downward salt and heat transport within the thermohaline staircases ($\gamma^{SF} < 1$).

Part of Antarctic Intermediate Water in the Great Australian Bight, known as Tasman Leakage[33], propagates westward towards the Agulhas region through the southern Indian Ocean[34,35]. Our results show that thermohaline staircases occur over the entire southern Indian Ocean (Fig. 1, red histograms in Fig. 4a) and that the characteristics of the thermohaline staircases change from east to west. In the east, the thermohaline staircases found contain more steps (Fig. 4b). However, the part of the water column that is susceptible to strong salt-fingering (71. 6° < Tu < 90° or $R_\rho > 2$, depths between thick white contour in Fig. 4a)[32] is relatively constant from east to west. This illustrates that strong salt fingering most likely occurs along this cross-section in the southern Indian Ocean.

Contribution to the ocean energy budget. To estimate the combined contribution of double-diffusive fluxes in thermohaline staircases to the global mechanical energy budget, we compute the average effective diffusivity of buoyancy in each detected interface based on the temperature and salinity steps between mixed layers[2,36]. A comparison between the characteristics of temperature and salinity steps found by the algorithm and those found in previous studies on thermohaline staircases indicated that the global dataset contains temperature and salinity steps of the correct magnitude in the salt-finger regime and provides an

upper bound for steps in the double-diffusive regime (see "Methods"). As the density flux ratio is different in the two regimes ($\gamma^{DC} > 1$ and $\gamma^{SF} < 1$), the effective diffusivities and thus their contributions to the global mechanical energy budget are computed separately.

To estimate the contribution of diffusive convection to the global mechanical energy budget, we compute the effective diffusivity of density with flux laws[37] (see "Methods"). This yields an upper bound for the average effective diffusivity of $K_\rho^{DC} = -1.47 \times 10^{-5}$ m^2 s^{-1} [-7.5×10^{-5} m^2 s^{-1}; -1.6×10^{-7} m^2 s^{-1}] (Fig. 2c). Next, we use this effective diffusivity to compute the dissipation (D^{DC}) from ref. [8], using their equation for the vertical fluxes through any depth level in the ocean:

$$D^{DC} = \Gamma^{-1} K_\rho^{DC} g A \Delta\rho, \tag{1}$$

where Γ is the mixing efficiency. We use standard values for the gravitational acceleration ($g = 9.8$ m s^{-2}), area of the ocean ($A = 3.6 \times 10^{14}$ m^2) and vertical density difference ($\Delta\rho = 1$ kg m^{-3})[8]. The mixing efficiency of double-diffusive mixing approaches $\Gamma = -1$, because it is driven by the release of potential energy and the production term of the turbulent kinetic energy budget becomes negligible[2,38]. In Eq. (1), ref. [8] assumes that the mixing in the ocean is evenly distributed. To account for the fact that thermohaline staircases do not occur everywhere (Fig. 1), we multiply Eq. (1) with the fraction of the staircase occurrence (n^{DC}). Moreover, because the depth of thermohaline staircases is variable[19], Eq. (1) is considered as an upper bound. Using these numbers, we obtain a
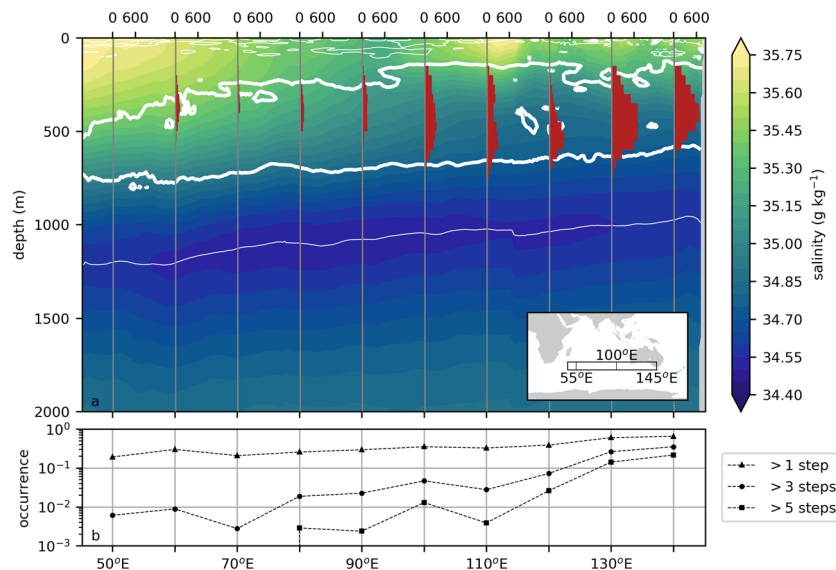
Fig. 4 Thermohaline staircases in the southern Indian Ocean. a Red histograms show the vertical distribution of number of detected mixed layers in thermohaline staircases per 10 degrees longitude. The thick (thin) white contour corresponds to Turner angles[32] of Tu = 71.6° (Tu = 45°), indicating the susceptibility of the water column to double diffusion in the salt-finger regime (45° < Tu < 90°). Background shading indicates the mean vertical salinity profile obtained from the World Ocean Atlas 2018[57]. The inlay shows the considered region: 45°E–145°E, 32°S–42°S. **b** Occurrence of number of steps per profile in per 10 degrees longitude (note the logarithmic vertical axis).

value of $D^{DC} = 3.3$ GW [0.0 GW; 16 GW] for dissipation by diffusive-convective thermohaline staircases.

We use a similar method to estimate the contribution of thermohaline staircases in the salt-finger regime to the dissipation (D^{SF}). However, because the flux laws based on laboratory experiments are known to overestimate salt-finger fluxes in the real ocean by an order of magnitude[39,40], we compute the effective diffusivity of buoyancy in the salt-finger regime based on an empirical estimate[31]. Using this estimate[31], we obtain an effective diffusivity of $K_\rho^{SF} = -1.47 \times 10^{-5}$ m^2 s^{-1} [-6.2×10^{-7} m^2 s^{-1}; -5.6×10^{-5} m^2 s^{-1}], which yield a contribution of salt fingers to the global mixing energetics of $D^{SF} = 4.2$ GW [0.2 GW; 18 GW]. Similar to the dissipation obtained in the diffusive-convective regime, this should be considered as an upper bound, because the depth of the thermohaline staircases is variable.

Our estimate for the total contribution of double diffusion to the global mechanical energy budget by diffusive convection and salt fingers combined thus adds up to $D = 7.5$ GW [0.1 GW; 32.8 GW]. Owing to the high mixing efficiency of double diffusion ($\Gamma = -1$) compared to turbulent mixing ($\Gamma^{turb} = 0.2$), double diffusion is able to mix five times more than down-gradient turbulence with the same amount of energy. Notably, the mixing by double diffusion restratifies the water column in contrast to the mixing by down-gradient turbulence. Consequently, double-diffusive mixing contributes to the mechanical energy necessary to maintain the stratification. Depending on its location, the double-diffusive mixing can thus either enhance the downwelling in regions with deep convection in the North Atlantic Ocean or it can prevent the upwelling at lower latitudes[2]. This implies that a part of the double-diffusive mixing in downwelling regions is already contained in the estimates for the amount of abyssal mixing that were previously computed[8]. Therefore, we conclude that the contribution of double-diffusive mixing to the global mechanical energy budget is limited.

Summary and global implications

In this study, we presented a global analysis of thermohaline staircases identified in profiles of Argo floats and Ice-Tethered Profilers. The global distribution of thermohaline staircases shows that thermohaline staircases are confined to specific regions determined by the local water-mass characteristics: thermohaline staircases in the diffusive-convective regime are predominantly found at high latitudes, while staircases in the salt-finger regime dominate at low latitudes. Our analysis revealed a new staircase region in the Great Australian Bight and southern Indian Ocean. As the waters in the southern Indian Ocean are likely to become more susceptible to double-diffusive mixing[10] and previous studies showed that double-diffusive fluxes in thermohaline staircases can modify water-mass characteristics[11,12], we speculate on the potential implications of this new staircase region.
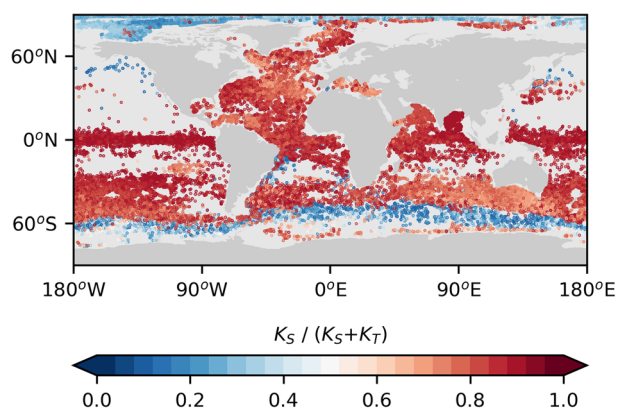
The thermohaline staircases in the southern Indian Ocean overlie the waters of the Tasman Leakage. As the salt content of the Tasman Leakage waters is considered to affect the stability of the Atlantic Meridional Overturning Circulation (AMOC)[35,41], the double-diffusive salt fluxes in this region might impact AMOC stability. This impact can be determined qualitatively by using an indicator of AMOC stability, usually referred to M_{ov}, measuring the freshwater transport of the AMOC at 35°S in the Atlantic[42–45]. When $M_{ov} > 0$, the AMOC transports salt out of the Atlantic and it is less sensitive to North Atlantic surface freshwater anomalies[42–45]. For $M_{ov} < 0$, the AMOC imports salt and can undergo transitions to a weak AMOC state due to the positive salt advection feedback. Further research is necessary to quantify whether stronger double-diffusive salt fluxes in a future climate[10] can increase the salt content of the Tasman Leakage waters and, consequently, have a destabilizing effect on the AMOC by changing the M_{ov}.

By analyzing the occurrence and properties of the thermohaline staircases, we also estimated the impact of double-diffusive mixing in this study. Of each thermohaline staircase, we estimated the effective diffusivity of buoyancy based on both flux laws (diffusive convection)[37] and empirical estimates (salt fingers)[31]. Although there are some uncertainties regarding the diffusivities obtained from these computations that most likely result in an overestimation of the magnitude of these diffusivities (see "Methods")[46,47], these computations are necessary to obtain an observationally based estimate of the contribution of double-diffusive mixing to the global mechanical energy

Table 1 Percentage of profiles with thermohaline staircases in the global dataset and dissipation computed for different input parameters of the detection algorithm[19].

Input	Occurrence (%)	D (GW)
MA: 50 dbar	14.3	8.2 [0.1; 34.4]
MA: 100 dbar	14.5	8.5 [0.1; 34.5]
MA: 300 dbar	13.9	6.4 [0.1; 28.1]
MA: 350 dbar	13.4	5.8 [0.1; 24.8]
$\partial\sigma_1/\partial p_{max} = 0.5 \times 10^{-4}\,\mathrm{kg\,m^{-3}\,dbar^{-1}}$	1.2	6.3 [0.0; 20.7]
$\partial\sigma_1/\partial p_{max} = 2.5 \times 10^{-4}\,\mathrm{kg\,m^{-3}\,dbar^{-1}}$	6.6	4.0 [0.0; 15.8]
$\partial\sigma_1/\partial p_{max} = 7.5 \times 10^{-4}\,\mathrm{kg\,m^{-3}\,dbar^{-1}}$	21.2	9.8 [0.2; 42.7]
$\partial\sigma_1/\partial p_{max} = 10 \times 10^{-4}\,\mathrm{kg\,m^{-3}\,dbar^{-1}}$	27.5	18.1 [0.3; 48.8]
$\Delta\sigma_{1,max} = 0.5 \times 10^{-3}\,\mathrm{kg\,m^{-3}}$	18.5	12.3 [0.2; 41.8]
$\Delta\sigma_{1,max} = 2.5 \times 10^{-3}\,\mathrm{kg\,m^{-3}}$	17.4	8.9 [0.2; 39.2]
$\Delta\sigma_{1,max} = 7.5 \times 10^{-3}\,\mathrm{kg\,m^{-3}}$	11.8	8.4 [0.1; 28.4]
$\Delta\sigma_{1,max} = 10 \times 10^{-3}\,\mathrm{kg\,m^{-3}}$	9.8	7.9 [0.1; 24.9]
$h_{max,IF} = 10$ dbar	14.1	7.2 [0.1; 31.6]
$h_{max,IF} = 20$ dbar	14.3	7.5 [0.1; 33.3]
$h_{max,IF} = 40$ dbar	11.4	5.2 [0.1; 23.4]
$h_{max,IF} = $ infinity	14.5	7.6 [0.1; 33.5]

One input variable is varied per computation compared to the standard setting (MA: moving average window; $\partial\sigma_1/\partial p_{max}$: threshold for mixed-layer density gradient; $\Delta\sigma_{1,max}$: maximum density difference over the extent of of the mixed-layer; $h_{max,IF}$: maximum interface height). The 2.5- and 97.5-percentile values are given between brackets.

Fig. 5 Relative magnitude of the effective diffusivity of salt compared to the combined effective diffusivities of heat and salt ($K_S/(K_S + K_T)$). Thermohaline staircases in the salt-finger regime ($K_S > K_T$) are denoted by red dots and thermohaline staircases in the diffusive convection regime ($K_T > K_S$) are denoted by blue dots.

budget. Using these values, we estimated an upper bound of the contribution of double-diffusive mixing to the global mechanical energy budget (7.5 GW [0.1 GW; 32.8 GW]), which is relatively small (<1%). The robustness of these results to different input variables of the detection algorithm that was used to obtain the global dataset is confirmed by a sensitivity analysis (Table 1). Hence we conclude that the direct effect of double-diffusive mixing to the maintenance of the abyssal stratification is negligible.

However, the global distribution of thermohaline staircases indicated that double-diffusive mixing is widespread. This implies that in a large part of the ocean the magnitudes of the effective diffusivity of heat and salt differ from each other. By including an inequality of these effective diffusivities in global ocean models based on the characteristics of thermohaline staircases, double-diffusive mixing can in principle be parameterized in ocean models (Fig. 5). Especially in regions with high-staircase occurrence, this is expected to yield more realistic model results on both regional and global scales.

Methods

We use the global dataset of thermohaline staircases that is obtained with an algorithm to automatically detect these structures[19]. In short, the staircase detection algorithm is applied on vertical temperature and salinity profiles obtained from Ice-Tethered Profilers and Argo Floats between 13 November 2001 and 14 May 2020. The data is obtained from http://www.whoi.edu/itp and http://www.argo.ucsd.edu for the Ice-Tethered Profilers and Argo floats, respectively. The average coverage is 1.4×10^{-3} observations in $\mathrm{km^{-2}}$ ($A_{ocean} \approx 3.6 \times 10^8\,\mathrm{km^{-2}}$), with the highest observation density of $2.5\,\mathrm{km^{-2}}$ in the Arctic Ocean (83°N and 99°W), and smallest observation density in the centers of the subtropical gyres (see Fig. 2 in ref. [19]). This variation in data coverage results in a (small) overestimate of the occurrence of diffusive-convective staircases as these predominantly occur at high latitudes. Moreover, the Arctic Ice-Tethered Profilers generally follow the ice floe and not the flow at the depth of the staircase, which results in a randomized field of staircase observations in this region. After a quality control, profiles that have an average resolution exceeding 5 dbar and contain observations below 500 dbar are selected, which results in a dataset consisting of 487,493 profiles. Their average vertical resolution is relatively high (finer than 2.5 dbar) in the upper 1000 m of the water column[19], where most thermohaline staircases are found[2]. Deeper in the water column, the average vertical resolution of the profiles is ~2.5 dbar. Afterwards, the profiles are subsequently linearly interpolated from 0 to 2000 dbar with a vertical resolution of 1 dbar. The algorithm itself consists of five steps that detect sequences of interfaces in each temperature and salinity profile:

1. Mixed layers are identified by selecting layers with density gradients below $5 \times 10^{-4}\,\mathrm{kg\,m^{-3}\,dbar^{-1}}$. Where this criterion is met, the mixed layers are defined as the layer within a density interval of $5 \times 10^{-3}\,\mathrm{kg\,m^{-3}}$.
2. The interfaces, defined as the layers between these mixed layers, should have larger temperature, salinity and density variations than those found within the adjacent mixed layers.
3. The interfaces are required to be thinner than the adjacent mixed layers, and the maximum interface thickness is limited to 30 dbar. Furthermore, interfaces are required to contain no temperature or salinity inversion.
4. The double-diffusive regime of each interface is determined: when the temperature and salinity of a mixed-layer below an interface are higher (lower) than the temperature and salinity of the mixed-layer directly above, the regime of the interface is classified as diffusive-convective (salt-finger) regime.
5. Sequences of interfaces that are of the same double-diffusive regime are detected; each sequence of interfaces consisting of more than one step (>2 mixed layers) is classified as a thermohaline staircase.

A detailed description of the algorithm to obtain this dataset and tests of its robustness can be found in ref. [19]. A sensitivity test performed for the chosen input parameters of the detection algorithm shows robust results[19]. As an example, the sensitivity of the occurrence of thermohaline staircases to the value of the mixed-layer criterion (step 1 of the algorithm) is shown in Fig. 6. It clearly shows that while it affects the number of detected steps, the same spatial pattern emerges. Owing to the vertical resolution of the observations and the linear interpolation by the algorithm, it cannot detect very thin interfaces[19]. This particularly plays a role
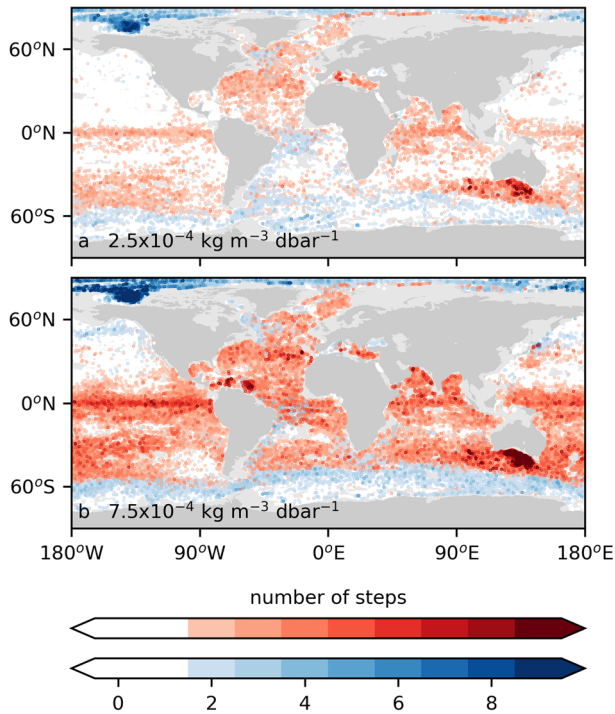
Fig. 6 Sensitivity of the number of staircases detected resulting for different input parameters of the staircase detection algorithm[19]. a $\partial\sigma_1/\partial p_{max} = 2.5 \times 10^{-4}\,\mathrm{kg\,m^{-3}\,dbar^{-1}}$ **b** $\partial\sigma_1/\partial p_{max} = 7.5 \times 10^{-4}\,\mathrm{kg\,m^{-3}\,dbar^{-1}}$. For each profile, the number of steps per staircase in the salt-finger regime (red dots) and diffusive-convective regime (blue dots) is plotted. Profiles with the largest numbers are plotted last for clarity. Figure 1 shows the same for the standard value of $\partial\sigma_1/\partial p_{max} = 5.0 \times 10^{-4}\,\mathrm{kg\,m^{-3}\,dbar^{-1}}$.

for staircases in the diffusive-convective regime in the Arctic Ocean, where interfaces can be as thin as 0.1 m[2,48]. The minimum layer height that can be detected by the algorithm is 2 dbar[19]. Consequently, the smallest interfaces are missed by the algorithm and the average temperature and salinity steps in the diffusive-convective interfaces are overestimated[19]. However, the algorithm detects an accurate staircase occurrence for staircases in the diffusive-convective regime (n^{DC}) in this region[19]. As thermohaline staircases in the salt-finger regime have larger vertical length scales and are, therefore, more easily detected by the algorithm, the staircase occurrence for staircases in the salt-finger regime (n^{SF}) is also considered reliable.

At each staircase interface, the effective diffusivities of heat (K_T), salt (K_S), and buoyancy (K_ρ) are computed. Taking into account that the detection algorithm mainly detects interfaces that arise from double-diffusive mixing[19], we assume that all detected interfaces result from either diffusive convection (DC) or from salt fingering (SF). To limit detection of thermohaline intrusions, the detection algorithm only detects sequences of interfaces within the same regime (step 5 of the algorithm) as intrusions induce interfaces that alternate in both different regimes[47]. Although it is expected that such intrusions have a limited impact on the results, the detection of thermohaline intrusions could result in an underestimation of the computed fluxes through an interface by 50%[47].

To compute the effective diffusivities in the diffusive-convective regime, we apply a similar flux law[49]. Although empirical evidence suggests that it is reasonable to extrapolate these flux laws to the oceanic environment, uncertainties do exist about the magnitude of most variables within these flux laws[50]. In general, the flux laws proposed by ref. [37] agree well with observations[15,16,51]; we therefore choose to apply these in this study. However, it should be noted that there are some indications, mainly from numerical simulations, that fluxes computed with these relations[37] could underestimate observed heat fluxes by 50%[46]. Following ref. [37], we compute the effective diffusivity of heat:

$$K_T^{DC} = e^{\frac{4.8}{R_\rho^{0.72}}} \left(\frac{\alpha g \kappa}{\mathrm{Pr}}\right)^{\frac{1}{3}} (\Delta T_{IF})^{\frac{4}{3}} \left(\frac{\partial T}{\partial z}\right)^{-1}, \tag{2}$$

where R_ρ is the density ratio ($R_\rho = \left(\alpha\frac{\partial T}{\partial z}\right)\left(\beta\frac{\partial S}{\partial z}\right)^{-1}$, which is limited to $0 < R_\rho < 1$), κ the molecular diffusivity of heat in $\mathrm{m^2\,s^{-1}}$, α the thermal expansion coefficient in $^\circ C^{-1}$, g the gravitational acceleration in $\mathrm{m\,s^{-2}}$, Pr the Prantle number and ΔT_{IF} the conservative temperature difference across an interface in $^\circ C$. The vertical gradients of conservative temperature are computed with a central differences scheme from

temperature profiles that are smoothed with a 50 dbar moving average. Recall that the average magnitude of the temperature differences across the interfaces is overestimated by the algorithm[19]. Therefore, the effective diffusivity should be considered as an upper bound. We convert the effective diffusivity of heat to heat fluxes (F_H) as: $F_H = \rho c_p K_T^{DC}\frac{\partial T}{\partial z}$, where ρ is a reference density and c_p the specific heat of seawater. The effective diffusivity of salt follows from the effective diffusivity of heat in combination with the flux ratio γ:

$$K_S^{DC} = K_T^{DC}\frac{R_\rho}{\gamma^{DC}}, \tag{3}$$

where the density flux ratio (γ) computed following Kelley[37] as:

$$\gamma^{DC} = \left(\frac{R_\rho^{-1} + 1.4\left(R_\rho^{-1} - 1\right)^{\frac{3}{2}}}{1 + 14\left(R_\rho^{-1}\right)^{\frac{3}{2}}}\right)^{-1}. \tag{4}$$

In contrast to the diffusive convection, the flux laws cannot be extrapolated to oceanic environments for thermohaline staircases in the salt-finger regime, as they are known to lead to a significant overestimation of the effective diffusivities[2,39,40,50]. Therefore, we use an empirical estimate[31] to compute the effective diffusivities of salt and heat instead:

$$K_S^{SF} = \left(\frac{135}{\left(R_\rho - 1\right)^{\frac{1}{2}}} - 62.75\right)\kappa R_\rho, \tag{5}$$

with a density ratio limit of $1 < R_\rho < 10$. The effective diffusivity of heat is computed as follows:

$$K_T^{SF} = K_S^{SF}\frac{\gamma^{SF}}{R_\rho}, \tag{6}$$

where γ^{SF} is computed as $\gamma^{SF} = 2.709e^{-2.513R_\rho} + 0.5128$[31]. Note that, in contrast to the diffusive-convective regime, the effective diffusivities in the salt-finger regime do not depend on the temperature or salinity jumps across the interfaces. A comparison of our results to tracer-based oceanic observations in the western tropical Atlantic Ocean[17] indicates that we obtained lower effective diffusivities than found in these observations (Fig. 2). However, because these observations most likely also include mixing in the vicinity of topography, these high estimates are most likely a combination of double-diffusive mixing and turbulent mixing. Finally, the effective diffusivity of buoyancy is computed separately for both regimes from the combined effective diffusivities of heat and salt:

$$K_\rho = -K_T\frac{1 - \gamma^{-1}}{R_\rho^{-1} - 1}. \tag{7}$$

Data availability

Code availability

References
1. Stern, M. E. The "Salt-Fountain" and thermohaline convection. *Tellus* **12**, 172–175 (1960).
2. Radko, T. *Double-Diffusive Convection* (Cambridge University Press, 2013).
3. Schmitt, R. W. Flux measurements on salt fingers at an interface. *J. Mar. Res.* **37**, 419–436 (1979).
4. Gargett, A. E. & Holloway, G. Sensitivity of the GFDL ocean model to different diffusivities for heat and salt. *J. Phys. Oceanogr.* **22**, 1158–1177 (1992).
5. Merryfield, W. J., Holloway, G. & Gargett, A. E. A global ocean model with double-diffusive mixing. *J. Phys. Oceanogr.* **29**, 1124–1142 (1999).
6. Oschlies, A., Dietze, H. & Kähler, P. Salt-finger driven enhancement of upper ocean nutrient supply. *Geophys. Res. Lett.* **30** https://doi.org/10.1029/2003GL018552 (2003).
7. Munk, W. H. Abyssal recipes. *Deep Sea Res. Oceanogr. Abstr.* **13**, 707–730 (1966).
8. Munk, W. & Wunsch, C. Abyssal recipes II: energetics of tidal and wind mixing. *Deep Sea Res. Oceanogr. Res. Pap.* **45**, 1977–2010 (1998).

9. Ferrari, R. & Wunsch, C. Ocean circulation kinetic energy: reservoirs, sources, and sinks. *Annual Review of Fluid Mechanics* **41**, 253–282 (2009).
10. Johnson, G. C. & Kearney, K. A. Ocean climate change fingerprints attenuated by salt fingering? *Geophys. Res. Lett.* **36**, https://doi.org/10.1029/2009GL040697 (2009).
11. Schroeder, K., Chiggiato, J., Bryden, H. L., Borghini, M. & BenIsmail, S. Abrupt climate shift in the western Mediterranean Sea. *Sci. Rep.* **6**, 23009 (2016).
12. Zodiatis, G. & Gasparini, G. P. Thermohaline staircase formations in the Tyrrhenian Sea. *Deep Sea Res. Oceanogr. Res. Pap.* **43**, 655–678 (1996).
13. Schmitt, R. W. Spice and the Demon. *Science* **283**, 498–499 (1999).
14. Chassignet, E. P. & Verron, J. (eds.) *Ocean Modeling and Parameterization* (Springer Netherlands, 1998).
15. Timmermans, M.-L., Toole, J., Krishfield, R. & Winsor, P. Ice-Tethered Profiler observations of the double-diffusive staircase in the Canada Basin thermocline. *J. Geophys. Res.* **113**, https://doi.org/10.1029/2008JC004829 (2008).
16. Shibley, N. C., Timmermans, M.-L., Carpenter, J. R. & Toole, J. M. Spatial variability of the Arctic Ocean's double-diffusive staircase. *J. Geophys. Res.* **122**, 980–994 (2017).
17. Schmitt, R. W. Enhanced diapycnal mixing by salt fingers in the thermocline of the tropical Atlantic. *Science* **308**, 685–688 (2005).
18. Guthrie, J. D., Fer, I. & Morison, J. H. Thermohaline staircases in the Amundsen Basin: possible disruption by shear and mixing. *J. Geophys. Res.* **122**, 7767–7782 (2017).
19. van der Boog, C. G., Koetsier, J. O., Dijkstra, H. A., Pietrzak, J. D. & Katsman, C. A. Global dataset of thermohaline staircases obtained from Argo floats and Ice-Tethered Profilers. *Earth Syst. Sci. Data* **13**, 43–61 (2021).
20. Padman, L. & Dillon, T. M. Thermal microstructure and internal waves in the Canada Basin diffusive staircase. *Deep Sea Res. Oceanogr. Res. Pap.* **36**, 531–542 (1989).
21. Muench, R. D., Fernando, H. J. S. & Stegen, G. R. Temperature and Salinity Staircases in the Northwestern Weddell Sea. *J. Phys. Oceanogr.* **20**, 295–306 (1990).
22. Polyakov, I. V. et al. Mooring-based observations of double-diffusive staircases over the Laptev Sea slope*. *J. Phys. Oceanogr.* **42**, 95–109 (2012).
23. Bebieva, Y. & Timmermans, M.-L. Double-diffusive layering in the Canada Basin: An explanation of along-layer temperature and salinity gradients. *J. Geophys. Res.* **124**, 723–735 (2019).
24. Bebieva, Y. & Speer, K. The regulation of sea ice thickness by double-diffusive processes in the ross gyre. *J. Geophys. Res.* **124**, 7068–7081 (2019).
25. Schmitt, R. W., Perkins, H., Boyd, J. D. & Stalcup, M. C. C-SALT: An investigation of the thermohaline staircase in the western tropical North Atlantic. *Deep Sea Res. Oceanogr. Res. Pap.* **34**, 1655–1665 (1987).
26. van der Boog, C. G. et al. Hydrographic and biological survey of a surface-intensified anticyclonic eddy in the Caribbean sea. *J. Geophys. Res.* **124**, 6235–6251 (2019).
27. Merryfield, W. J. Origin of thermohaline staircases. *J. Phys. Oceanogr.* **30**, 1046–1068 (2000).
28. Tait, R. I. & Howe, M. R. Thermohaline staircase. *Nature* **231**, 178–179 (1971).
29. Durante, S. et al. Permanent thermohaline staircases in the Tyrrhenian Sea. *Geophys. Res. Lett.* **46**, 1562–1570 (2019).
30. Lee, C., Chang, K.-I., Lee, J. H. & Richards, K. J. Vertical mixing due to double diffusion in the tropical western Pacific. *Geophys. Res. Lett.* **41**, 7964–7970 (2014).
31. Radko, T. & PaulSmith, D. Equilibrium transport in double-diffusive convection. *J. Fluid Mech.* **692**, 5–27 (2012).
32. Ruddick, B. A practical indicator of the stability of the water column to double-diffusive activity. *Deep Sea Res. Oceanogr. Res. Pap.* **30**, 1105–1107 (1983).
33. Speich, S. et al. Tasman leakage: A new route in the global ocean conveyor belt. *Geophys. Res. Lett.* **29**, https://doi.org/10.1029/2001GL014586 (2002).
34. Drijfhout, S. S. The origin of Intermediate and Subpolar Mode Waters crossing the Atlantic equator in OCCAM. *Geophys. Res. Lett.* **32**, L06602 (2005).
35. Speich, S., Blanke, B. & Cai, W. Atlantic meridional overturning circulation and the Southern Hemisphere supergyre. *Geophys. Res. Lett.* **34**, https://doi.org/10.1029/2007GL031583 (2007).
36. Nakano, H. & Yoshida, J. A note on estimating eddy diffusivity for oceanic double-diffusive convection. *J. Oceanogr.* **75**, 375–393 (2019).
37. Kelley, D. E. Fluxes through diffusive staircases: a new formulation. *J. Geophys. Res.* **95**, https://doi.org/10.1029/JC095iC03p03365 (1990).
38. Osborn, T. R. Estimates of the local rate of vertical diffusion from dissipation measurements. *J. Phys. Oceanogr.* **10**, 83–89 (1980).
39. Taylor, J. R. & Veronis, G. Experiments on double-diffusive sugar-salt fingers at high stability ratio. *J. Fluid Mech.* **321**, 315–333 (1996).
40. Radko, T. What determines the thickness of layers in a thermohaline staircase? *J. Fluid Mech.* **523**, 79–98 (2005).
41. Gordon, A. L. The brawniest retroflection. *Nature* **421**, 904–905 (2003).
42. Rahmstorf, S. On the freshwater forcing and transport of the Atlantic thermohaline circulation. *Clim. Dyn.* **12**, 799–811 (1996).
43. de Vries, P. & Weber, S. L. The Atlantic freshwater budget as a diagnostic for the existence of a stable shut down of the meridional overturning circulation. *Geophys. Res. Lett.* **32**, https://doi.org/10.1029/2004GL021450 (2005).
44. Dijkstra, H. A. Characterization of the multiple equilibria regime in a global ocean model. *Tellus A* **59**, 695–705 (2007).
45. Castellana, D., Baars, S., Wubs, F. W. & Dijkstra, H. A. Transition probabilities of noise-induced transitions of the Atlantic Ocean circulation. *Sci. Rep.* **9**, 20284 (2019).
46. Flanagan, J. D., Lefler, A. S. & Radko, T. Heat transport through diffusive interfaces. *Geophys. Res. Lett.* **40**, 2466–2470 (2013).
47. Bebieva, Y. & Timmermans, M.-L. The relationship between double-diffusive intrusions and staircases in the Arctic Ocean. *J. Phys. Oceanogr.* **47**, 867–878 (2017).
48. Padman, L. & Dillon, T. M. Vertical heat fluxes through the Beaufort Sea thermohaline staircase. *J. Geophys. Res.* **92**, https://doi.org/10.1029/JC092iC10p10799 (1987).
49. Turner, J. S. The coupled turbulent transports of salt and heat across a sharp density interface. *Int. J. Heat. Mass Transf.* **8**, 759–767 (1965).
50. Kelley, D. E., Fernando, H. J. S., Gargett, A. E., Tanny, J. & Özsoy, E. The diffusive regime of double-diffusive convection. *Double-Diffus. Oceanogr.* **56**, 461–481 (2003).
51. Robertson, R., Padman, L. & Levine, M. D. Fine structure, microstructure, and vertical mixing processes in the upper ocean in the western Weddell Sea. *J. Geophys. Res.* **100**, https://doi.org/10.1029/95JC01742 (1995).
52. van der Boog, C. G., Koetsier, J. O., Dijkstra, H. A., Pietrzak, J. D. & Katsman, C. A. Data supplement for 'global dataset of thermohaline staircases obtained from argo floats and ice-tethered profilers'. *Zenodo* (SEANOE, 2020).
53. Krishfield, R., Toole, J., Proshutinsky, A. & Timmermans, M.-L. Automated Ice-Tethered Profilers for seawater observations under pack ice in all seasons. *J. Atmos. Ocean. Technol.* **25**, 2091–2105 (2008).
54. Toole, J. M., Krishfield, R., Timmermans, M.-L. & Proshutinsky, A. The ice-tethered profiler: argo of the Arctic. *Oceanography* **24**, 126–135 (2011).
55. Argo. *Argo float data and metadata from Global Data Assembly Centre* (Argo GDAC, 2020).
56. Amante, C. and B.W. Eakins, ETOPO1 1 Arc-Minute Global Relief Model: Procedures, Data Sources and Analysis. NOAA Technical Memorandum NESDIS NGDC-24. https://doi.org/10.7289/V5C8276M (National Geophysical Data Center, NOAA 2009).
57. Zweng, M. M. et al. *World Ocean Atlas 2018, Volume 2: Salinity*. Technical report, Mishonov Technical ed. (NOAA Atlas NESDIS 82, 2019).

Acknowledgements

Author contributions

C.v.d.B. and H.D. conceived the idea of the study. C.v.d.B. performed the analysis and wrote the manuscript. C.K., J.P., and H.D. contributed to the discussion and assisted in writing the manuscript.

Competing interests

The authors declare no competing interests.

Additional information

Supplementary information The online version contains supplementary material available at https://doi.org/10.1038/s43247-021-00113-x.

Correspondence and requests for materials should be addressed to C.G.v.d B.

Peer review information Primary handling editor: Heike Langenberg.

Reprints and permission information is available at http://www.nature.com/reprints

Publisher's note Springer Nature remains neutral with regard to jurisdictional claims in published maps and institutional affiliations.